

Analytical solutions for the surface- and orientation-averaged SERS enhancement factor of small plasmonic particles

Nikolai G. Khlebtsov^{1,2}  | Eric C. Le Ru³

¹Institute of Biochemistry and Physiology of Plants and Microorganisms, Russian Academy of Sciences, Saratov, Russia

²Faculty of Nano- and Biomedical Technologies, Saratov State University, Saratov, Russia

³The MacDiarmid Institute for Advanced Materials and Nanotechnology, School of Chemical and Physical Sciences, Victoria University of Wellington, Wellington, New Zealand

Correspondence

Nikolai G. Khlebtsov, Institute of Biochemistry and Physiology of Plants and Microorganisms, Russian Academy of Sciences, 13 Prospekt Entuziastov, Saratov 410049, Russia.

Email: khlebtsov@ibppm.ru

Funding information

Russian Foundation of Basic Research, Grant/Award Number: 18-52-7803; Russian Scientific Foundation, Grant/Award Number: 18-14-00016

Abstract

We derive analytical expressions for the surface- and orientation-averaged surface enhanced Raman scattering factor (SERS EF) for small plasmonic spheroids. These expressions are derived taking into account the Stokes shift and are shown to result in very different EFs to those in the $|E|^4$ -approximation for experimentally relevant parameters. The optical properties of spheroids are treated in terms of the common and improved electrostatic approximations (EA and IEA). The latter is newly introduced here and includes radiative damping, depolarization effects, and interactions with higher order multipoles, thus giving perfect agreement with exact T-matrix calculations of far-field cross sections and near-field SERS EFs over a much wider range of sizes. These accurate analytical expressions will be particularly relevant to SERS experiments in colloidal solutions where surface averaging (because of random molecular adsorption) and particle orientation averaging must both be taken into account. Comparison with recent experimental data and simulations for cigar-like particles show that the spheroid model tends to overestimate the SERS EF because of the higher curvature at the tips. Possible ways to generalize the analytic solution to other axially symmetrical particles are discussed.

KEY WORDS

electrostatic approximation, orientation averaging, plasmon resonance, SERS enhancement factor, surface enhanced Raman scattering (SERS), surface averaging, T-matrix

1 | INTRODUCTION

Raman spectroscopy is a powerful analytical tool for the study of molecules and their local environment in condensed phases, giving unique information about molecular vibration modes. However, the Raman scattering cross section is too small ($10^{-30} - 10^{-24}\text{cm}^2/\text{sr}$) for practical use in the same way as fluorescent dyes, which have cross section of about $10^{-16}\text{cm}^2/\text{sr}$.^[1] This explains why Raman spectroscopy has only found wide application after the discovery of the possible enormous

enhancement by metal nanostructures,^[2–4] the development of technologies for fabrication of plasmonic nanoparticles with desired properties,^[5] and notable progress in Raman spectrometers available on the market. As a result, a new scientific field—surface enhanced Raman scattering (SERS)—has been established, and the present and future of SERS was discussed recently.^[6]

The main mechanism of SERS is the enhancement of local electromagnetic (EM) fields under resonance plasmonic excitation.^[7] An additional chemical SERS enhancement^[8] may also arise from charge transfer

interactions between Raman molecules and plasmonic particles and its contribution is generally small compared with the EM one. Although the EM mechanism has been recognized for a long time,^[9] the interplay between the near-field SERS response and far-field properties of plasmonic structures is still far from being completely understood. For example, significant discrepancies between the theoretically predicted and measured dependences of the SERS enhancement factors with the aspect ratio or the localized plasmon resonance (LPR) wavelength have recently been reported for Au nanorods (AuNRs) functionalized with 1,4-nitrobenzenethiol (NBT).^[10] Existing synthesis protocols^[11–13] allow fabrication of high-quality AuNRs with finely controlled geometrical parameters and longitudinal LPR wavelength from vis to NIR. Moreover, by chemical etching of long AuNRs,^[14] it is possible to tune their LPR wavelength with accuracy of about 1 nm.^[15] This makes AuNRs a convenient experimental model to correlate SERS response with plasmonic properties of nanoparticles in colloids^[16] and in single-particle experiments.^[17]

The SERS enhancement consist of the plasmonic local-field enhancement at the laser frequency ω_L , $M_{loc}(\omega_L) \sim |\mathbf{E}_{loc}(\omega_L)|^2$, and the enhanced scattering of dipole radiation (DR) emitted at the Raman-shifted frequency ω_R , $M_{Rad}(\omega_R)$. The resultant SERS EF is $EF = M_{loc}(\omega_L)M_{Rad}(\omega_R)$. The first contribution is given by solution of a plane wave (PW) electromagnetic problem. For the second contribution, the source is the dipole located near a plasmonic particle. This problem can be solved with the dipole Green function.^[18] Another approach to the rigorous treatment of the DR contribution is based on the optical reciprocity theorem (ORT),^[19] which avoids Green function singularities by consideration of two specific PW problems. Because of optical reciprocity,^[19] the DR enhancement $M_{Rad}(\omega_R)$ can in general be approximated by $|\mathbf{E}_{loc}(\omega_R)|^2$. Although this approximation formally looks as the PW enhancement at the Raman-shifted frequency, the ORT clearly demonstrates that in fact it is an approximation for quite a different DR problem. Thus, owing to optical reciprocity,^[19] the total SERS enhancement can be approximated by the product of the local-field intensities $|\mathbf{E}_{loc}(\omega)|^2|\mathbf{E}_{loc}(\omega_R)|^2$, where the second term $|\mathbf{E}_{loc}(\omega_R)|^2$ takes into account the interaction between the emission from the excited dipole molecule and the plasmonic particle, as required^[18,20] and as explained in more detail elsewhere.^[21,22] This approximation still makes a number of assumptions, in particular neglecting the tensorial nature of the Raman process, and therefore the field polarization and molecular orientation effects.^[22,23] This approximation nevertheless provides the best

theoretical estimate to compare to experiments, especially given that tensorial aspects are hard to quantify experimentally.^[23,24]

For nonspherical particles in colloidal solution, the SERS enhancement factor should be averaged over the particle surface and orientations and possibly over the particle size and shape distributions. Although such calculations can be done numerically with finite-difference time-domain (FDTD) methods or finite element modeling (FEM), this is not an optimal strategy for multiple simulations aimed, for example, at the rational design of the most efficient SERS tags. Therefore, it would be desirable to have a simple yet accurate analytical solution for the surface- and orientation-averaged SERS enhancement factor $\langle EF \rangle = \langle |\mathbf{E}_{loc}(\omega)|^2 |\mathbf{E}_{loc}(\omega_R)|^2 \rangle$.

In this work, we derive new analytical expressions for this surface- and orientation-averaged EF for spheroidal particles. The local-field properties on the particle surface are calculated either within the common electrostatic approximation (EA)^[25] or using a novel improved electrostatic approximation (IEA),^[26] which includes radiative damping, depolarization effects, and interactions with higher order multipoles, thus giving excellent agreement with exact T-matrix solutions^[27] over a much wider range of particle size. The results are also compared with more realistic cigar-like particle model, calculated from surface integral equation (SIE)^[28,29] simulations.

2 | ANALYTICAL SOLUTIONS FOR THE AVERAGED ENHANCEMENT FACTORS

2.1 | Electrostatic approximation (EA)

We consider a prolate spheroidal particle with half axes (b, b, a) as shown schematically in Figure 1; the symmetry axis $a > b$ is directed along the z -axis of the particle frame (here, we follow the definitions in Majic et al.,^[26] which

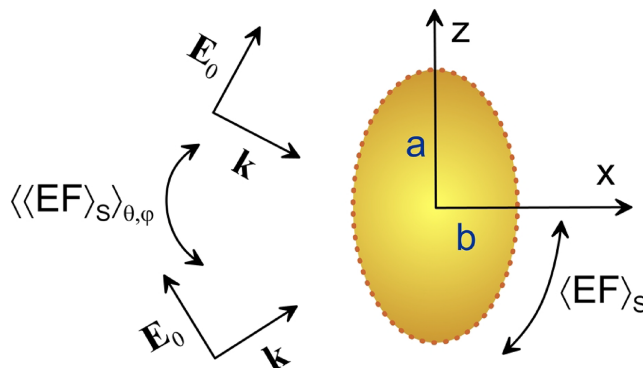


FIGURE 1 Schematics of the problem under consideration

differs from that in the book [Le Ru and Etchegoin^[21]] where the symmetry axis is directed along the x -axis). Our goal is to calculate the averaged SERS EF:

$$\langle EF_S \rangle = \left\langle \frac{1}{S} \int |\mathbf{E}_{loc}(\omega_L)|^2 |\mathbf{E}_{loc}(\omega_R)|^2 dS \right\rangle = \left\langle \langle |\mathbf{E}_{loc}(\omega_L)|^2 |\mathbf{E}_{loc}(\omega_R)|^2 \rangle_S \right\rangle, \quad (1)$$

where the outer angular brackets designate the averaging over orientations of particles or, equivalently in the EA, over the incident field polarization; the inner angular brackets with the subscript S stand for the averaging over the particle surface; and ω_L and ω_R are the excitation laser and Raman-shifted angular frequencies, respectively. Because of the strong spectral dependence of the local-field intensity on the excitation frequency, we do not simplify Equation 1 by using the approximation $\omega_R = \omega_L$, which would lead to the known four-power law $EF \sim |\mathbf{E}_{loc}(\omega_L)|^4$.

The local near-field is defined as the sum of the incident field and the plasmonic field \mathbf{E}_p at an arbitrary point \mathbf{r}_p near the particle surface. The electric vector of the incident light can be decomposed along the main symmetry axes (x, y, z) $\mathbf{E}_0 = E_{0x}\mathbf{e}_x + E_{0y}\mathbf{e}_y + E_{0z}\mathbf{e}_z$. For simplicity, we set $|\mathbf{E}_0| = 1$, and then $E_{0x,y,z}$ are the direction cosines of the vector \mathbf{E}_0 along the corresponding axes. We define $\kappa_i \equiv \kappa_{i\xi} = (\mathbf{e}_i \cdot \mathbf{e}_\xi)$, $i = x, y, z$, where the unit vector \mathbf{e}_ξ corresponds to the spheroidal coordinate system (ξ, η, ζ) ; that is, it is the outgoing normal to the spheroid surface. Then κ_i are the directional cosines with respect to the particle frame. For an arbitrary vector \mathbf{e}_ξ , we have

$$\sum_{i=x,y,z} \kappa_i^2 = 1. \quad (2)$$

Consider the surface average quantity

$$\langle \kappa_z^2 \kappa_y^2 \rangle_S = \langle \kappa_z^2 (1 - \kappa_z^2 - \kappa_x^2) \rangle_S = \langle \kappa_z^2 - \kappa_z^4 - \kappa_z^2 \kappa_x^2 \rangle_S. \quad (3)$$

By symmetry $\langle \kappa_z^2 \kappa_y^2 \rangle_S = \langle \kappa_z^2 \kappa_x^2 \rangle_S$, therefore,

$$\langle \kappa_z^2 \kappa_y^2 \rangle_S = \left\langle \frac{1}{2} (\kappa_z^2 - \kappa_z^4) \right\rangle_S. \quad (4)$$

Similarly,

$$\begin{aligned} \langle \kappa_x^2 \kappa_y^2 \rangle_S &= \langle \kappa_x^2 (1 - \kappa_x^2 - \kappa_z^2) \rangle_S = \langle \kappa_x^2 - \kappa_x^2 \kappa_z^2 - \kappa_x^4 \rangle_S \\ &= \left\langle \kappa_x^2 - \frac{1}{2} \kappa_z^2 + \frac{1}{2} \kappa_z^4 - \kappa_x^4 \right\rangle_S. \end{aligned} \quad (5)$$

Thus, all surface-averaged quantities are expressed in terms of $\langle \kappa_i^n \rangle_S$, $n = 2, 4$; $i = x, z$. The surface average

quantities $\langle \kappa_i^n \rangle_S$ have been calculated analytically^[21] for $n = 2, 4$:

$$\langle \kappa_z^2 \rangle_S = \frac{1 - e_p^2 f_p - 1}{e_p^2 f_p + 1}, \quad (6)$$

$$\langle \kappa_x^2 \rangle_S = \langle \kappa_y^2 \rangle_S = \frac{1}{2e_p^2} \frac{1 - (1 - 2e_p^2)f_p}{f_p + 1}, \quad (7)$$

$$f_p = \frac{\arcsin(e_p)}{e_p \sqrt{1 - e_p^2}}, \quad (8)$$

$$\langle \kappa_x^4 \rangle_S = \frac{1 - e_p^2 3 - e_p^2 - 3(1 - e_p^2)f_p}{e_p^4 f_p + 1}, \quad (9)$$

$$\langle \kappa_y^4 \rangle_S = \frac{3 - 2e_p^2 - (3 - 4e_p^2)f_p}{8e_p^4 f_p + 1}. \quad (10)$$

e_p is the prolate spheroid eccentricity

$$e_p = e_{prolate} = \sqrt{1 - \frac{b^2}{a^2}}. \quad (11)$$

Similar expressions can be derived for oblate spheroids ($a = b \geq c$) with eccentricity $e_o = e_{oblate} = \sqrt{1 - c^2/a^2}$.

Consider now the decomposition of the local near-field at the spheroid surface in the electrostatic approximation (EA) (see eq G.20 in Le Ru and Etchegoin^[21]):

$$\mathbf{E}_{loc} = \sum_{i=x,y,z} E_{oi} (a_i \mathbf{e}_i + b_i \kappa_i \mathbf{e}_\xi), \quad (12)$$

$$a_i = 1 - 3L_i \beta_i, \quad b_i = 3\beta_i. \quad (13)$$

β_i are the normalized polarizabilities along the main axes

$$\beta_i = \frac{\epsilon_r - 1}{3 + 3L_i(\epsilon_r - 1)}, \quad \epsilon_r = \epsilon/\epsilon_m. \quad (14)$$

ϵ and ϵ_m are the dielectric functions or the dielectric permittivities of spheroids and the surrounding medium, respectively; $L_{a,b}$ are the geometrical depolarization factors^[25]:

$$L_z = L_a = \frac{1-e_p^2}{e_p^2} \left(-1 + \frac{1}{2e_p} \ln \frac{1+e_p}{1-e_p} \right), L_{x,y} = L_b = (1-L_a)/2. \quad (15)$$

Let us calculate $|\mathbf{E}_{loc}|^2$ first

$$|\mathbf{E}_{loc}|^2 = \sum_i E_{oi}^2 (A_i + B_i \kappa_i^2) + \sum_{i \neq j} E_{oi} E_{oj} B_{ij} \kappa_i \kappa_j, \quad (16)$$

$$\text{where } A_i = |a_i|^2, \quad B_{ij} = b_i b_j^* + a_i b_j^* + a_j^* b_i, \quad (17)$$

$$B_i \equiv B_{ii} = |b_i|^2 + 2\text{Re}(a_i b_i^*) = |a_i + b_i|^2 - |a_i|^2. \quad (18)$$

Due to the Hermitian property $B_{ij} = B_{ji}^*$ and to the symmetry of $E_{oi} E_{oj} \kappa_i \kappa_j$ with respect to i, j indexes, the sum in Equation 16 is a real quantity, as it should be. After surface averaging of Equation 16, we have $\langle \kappa_i \kappa_j \rangle_S = 0$, $i \neq j$ and consequently

$$\langle |\mathbf{E}_{loc}(\omega)|^2 \rangle_S = \sum_i E_{oi}^2 (A_i + B_{ii} \langle \kappa_i^2 \rangle_S). \quad (19)$$

Now we proceed to $\langle |\mathbf{E}_{loc}(\omega)|^4 \rangle_S$, the SERS EF for zero-Stokes shift. From Equation 16, we have

$$\begin{aligned} |\mathbf{E}_{loc}(\omega)|^4 &= \left| \sum_i E_{oi}^2 (A_i + B_i \kappa_i^2) + \sum_{i \neq j} E_{oi} E_{oj} B_{ij} \kappa_i \kappa_j \right|^2 = \\ &= \left| \sum_i E_{oi}^2 (A_i + B_i \kappa_i^2) \right|^2 + 2\text{Re} \sum_i E_{oi}^2 (A_i + B_i \kappa_i^2) \sum_{m \neq n} E_{om} E_{on} B_{mn} \kappa_m \kappa_n \\ &+ \sum_{\substack{i \neq j \\ m \neq n}} E_{oi} E_{oj} E_{om} E_{on} B_{ij} B_{mn} \kappa_i \kappa_j \kappa_m \kappa_n. \end{aligned} \quad (20)$$

Performing the surface and orientation averaging of the first term, we arrive at the following result:

$$\begin{aligned} \langle \langle |\mathbf{E}_{loc}(\omega)|^4 \rangle_S \rangle^{(1)} &= \frac{1}{5} \sum_i (A_i^2 + 2A_i B_i \langle \kappa_i^2 \rangle_S + B_i^2 \langle \kappa_i^4 \rangle_S) + \\ &+ \frac{2}{15} \sum_{i < j} (A_i A_j + A_i B_j \langle \kappa_j^2 \rangle_S + A_j B_i \langle \kappa_i^2 \rangle_S + B_i B_j \langle \kappa_i^2 \kappa_j^2 \rangle_S), \end{aligned} \quad (21)$$

where the orientation-averaged quantities $\langle E_{oi}^4 \rangle = 1/5$, $\langle E_{oi}^2 E_{oj}^2 \rangle = 1/15$, and the symmetry properties over i, j indexes have been used. We then consider the second term in Equation 20. It can be shown that the

surface-averaged result equals zero. Indeed, κ_i^2 is an even function of the azimuthal angle φ (see eq G34 in Le Ru and Etchegoin^[21]), whereas $\kappa_m \kappa_n$ is an odd function of φ for $m \neq n$. Therefore,

$$\langle \kappa_i^2 \kappa_m \kappa_n \rangle_S = 0 \text{ for any } i \text{ and } m \neq n. \quad (22)$$

We are therefore left to calculate the last cross-term:

$$\sum_{\substack{i \neq j \\ m \neq n}} E_{oi} E_{oj} E_{om} E_{on} B_{ij} B_{mn} \langle \kappa_i \kappa_j \kappa_m \kappa_n \rangle_S. \quad (23)$$

We have 36 combinations of $\kappa_i \kappa_j \kappa_m \kappa_n$. However, there are only three non-zero average quantities $\langle \kappa_i^2 \kappa_j^2 \rangle_S, i \neq j$: $\langle \kappa_x^2 \kappa_y^2 \rangle_S, \langle \kappa_x^2 \kappa_z^2 \rangle_S, \langle \kappa_y^2 \kappa_z^2 \rangle_S$. The surface average of all other combinations equals zero. Thus, the remaining non-zero cross-terms are

$$\langle \langle |\mathbf{E}_{loc}|^4 \rangle_S \rangle^{(2)} = \sum_{i < j = 2, 3} E_{oi}^2 E_{oj}^2 (B_{ij}^2 + 2B_{ij} B_{ji} + B_{ji}^2) \langle \kappa_i^2 \kappa_j^2 \rangle_S. \quad (24)$$

Owing to Hermitian property,

$$B_{ij}^2 + 2B_{ij} B_{ji} + B_{ji}^2 = (B_{ij} + B_{ji})^2 = (B_{ij} + B_{ij}^*)^2 = 4(\text{Re}(B_{ij}))^2. \quad (25)$$

Thus, after orientation averaging, we obtain

$$\langle \langle |\mathbf{E}_{loc}|^4 \rangle_S \rangle = \frac{4}{15} \sum_{i < j = 2, 3} [\text{Re}(B_{ij})]^2 \langle \kappa_i^2 \kappa_j^2 \rangle_S. \quad (26)$$

Finally, the full expression for the surface- and orientation-averaged EF for zero-Stokes shift in the EA reads

$$\langle \langle |\mathbf{E}_{loc}(\omega)|^4 \rangle_S \rangle = \langle \langle |\mathbf{E}_{loc}(\omega)|^4 \rangle_S \rangle^{(1)} + \frac{4}{15} \sum_{i < j = 2, 3} [\text{Re}(B_{ij})]^2 \langle \kappa_i^2 \kappa_j^2 \rangle_S, \quad (27)$$

where the first term in Equation 27 is given by Equation 21.

Now one has to generalize the above derivation for non-zero Raman shift, when the fourth-power approximation is not valid. Without going into the full details, Equation 21 can be generalized to

$$\begin{aligned} \left\langle \langle |\mathbf{E}_{loc}(\omega_L)|^2 |\mathbf{E}_{loc}(\omega_R)|^2 \rangle_S \right\rangle^{(1)} = & \frac{1}{5} \sum_i \left[A_i^L A_i^R + (A_i^L B_i^R + A_i^R B_i^L) \langle \kappa_i^2 \rangle_S + B_i^L B_i^R \langle \kappa_i^4 \rangle_S \right] + \\ & \frac{1}{15} \sum_{i \neq j} \left(A_i^L A_j^R + A_i^L B_j^R \langle \kappa_j^2 \rangle_S + A_j^R B_i^L \langle \kappa_i^2 \rangle_S + B_i^L B_j^R \langle \kappa_i^2 \kappa_j^2 \rangle_S \right) \end{aligned} \quad (28)$$

Similarly, Equation 26 can be generalized to

$$\begin{aligned} \left\langle \langle |\mathbf{E}_{loc}(\omega_L)|^2 |\mathbf{E}_{loc}(\omega_R)|^2 \rangle_S \right\rangle^{(2)} = & \\ \frac{1}{15} \sum_{i < j=2,3} & [B_{ij}(\omega_L) B_{ij}(\omega_R) + B_{ij}(\omega_L) B_{ji}(\omega_R) + B_{ji}(\omega_L) B_{ij}(\omega_R) + B_{ji}(\omega_L) B_{ji}(\omega_R)] \langle \kappa_i^2 \kappa_j^2 \rangle_S = \\ \frac{4}{15} \sum_{i < j=2,3} & \operatorname{Re}[B_{ij}(\omega_L)] \operatorname{Re}[B_{ij}(\omega_R)] \langle \kappa_i^2 \kappa_j^2 \rangle_S, \end{aligned} \quad (29)$$

$$B_{ij}(\omega_W) \equiv B_{ij}^W = b_i^W b_j^{W*} + a_i^W b_j^{W*} + a_j^{W*} b_i^W, W = L, R. \quad (30)$$

The surface- and orientation-averaged SERS enhancement factor therefore reads

$$\begin{aligned} \langle EF \rangle = & \left\langle \langle |\mathbf{E}_{loc}(\omega_L)|^2 |\mathbf{E}_{loc}(\omega_R)|^2 \rangle_S \right\rangle = \\ \left\langle \langle |\mathbf{E}_{loc}(\omega_L)|^2 |\mathbf{E}_{loc}(\omega_R)|^2 \rangle_S \right\rangle^{(1)} + & \left\langle \langle |\mathbf{E}_{loc}(\omega_L)|^2 |\mathbf{E}_{loc}(\omega_R)|^2 \rangle_S \right\rangle^{(2)} \end{aligned} \quad (31)$$

By using symmetry properties, Equation 31 can be rewritten in the following form:

$$\begin{aligned} \langle \langle EF \rangle_S = & \left\langle \langle |\mathbf{E}_{loc}(\omega_L)|^2 |\mathbf{E}_{loc}(\omega_R)|^2 \rangle_S \right\rangle = \frac{1}{5} \sum_i G_{ii}^{LR} + \frac{1}{15} \sum_{i < j} (G_{ij}^{LR} + G_{ji}^{RL}) + \\ & \frac{4}{15} \sum_{i < j=2,3} \operatorname{Re}[B_{ij}(\omega_L)] \operatorname{Re}[B_{ij}(\omega_R)] \langle \kappa_i^2 \kappa_j^2 \rangle_S \end{aligned} \quad (32)$$

In Equation 32, the quantities G_{ij}^{LR} obey the symmetry $G_{ij}^{LR} = G_{ji}^{RL}$ and are defined by the following expression:

$$G_{ij}^{LR} = A_i^L A_j^R + A_i^L B_j^R \langle \kappa_j^2 \rangle_S + A_j^R B_i^L \langle \kappa_i^2 \rangle_S + B_i^L B_j^R \langle \kappa_i^2 \kappa_j^2 \rangle_S, \quad (33)$$

where

$$A_i^{L,R} = |a_i(\omega_{L,R})|^2, \quad (34)$$

$$B_{ij}^{L,R} = b_i(\omega_L) b_j^*(\omega_R) + a_i(\omega_L) b_j^*(\omega_R) + a_j^*(\omega_R) b_i(\omega_L) \quad (35)$$

$$B_i^{L,R} \equiv B_{ii}^{L,R} = |b_i|^2 + 2\operatorname{Re}(a_i b_i^*) = |a_i + b_i|^2 - |a_i|^2, \quad (36)$$

$$a_i(\omega) = 1 - 3L_i \beta_i(\omega), b_i(\omega) = 3\beta_i(\omega), \omega = \omega_{L,R}, \quad (37)$$

the indexes L and R stand for laser and Raman-shifted frequencies. These equations should be complemented by Equations 4 to 10 given earlier.

2.2 | Improved electrostatic approximation (IEA)

The T-matrix framework^[30] provides an exact solution to the EM scattering problem, from which the SERS enhancement can be derived. The T-matrix itself is a generalization of the concept of polarizability to higher orders.^[31] For a spheroid of revolution around the z -axis, its lowest-order elements correspond to the dipolar polarizability along the two main axes: $T_{11,m=0}^{22}$ is proportional to the dipolar polarizability along the z -axis, whereas $T_{11,m=1}^{22}$ corresponds to that along the x - and y -axes.^[26,31] These T-matrix elements represent the exact dipolar response of the particle, including radiative damping, depolarization effects, and interactions with higher order multipoles. In Majic et al.,^[26] we derived Taylor expansions for these generalized polarizabilities in terms of the size parameter $X = 2\pi\sqrt{\epsilon_m}(a/\lambda)$. The resulting analytical approximations are correct up to terms of order X^6 . Here, we propose to use these improved dipolar polarizability expressions in a standard EA model to formulate an improved EA (IEA) model for the calculation of the surface- and orientation-averaged SERS EF. The modified polarizabilities α_i of the IEA are deduced from the Taylor expansions of Majic et al.^[26] and are defined by the following expressions:

$$\alpha_i = \beta_i \frac{1}{1 - \Omega_i X^2 - i \frac{2}{3h^2} \beta_i X^3} \quad (38)$$

where $h = a/b$ is the aspect ratio and

$$\Omega_z = \frac{9e_p^2}{25} + \frac{\epsilon_r(1 - e_p^2) - 2}{5[1 + (\epsilon_r - 1)L_z]}, \quad (39)$$

$$\Omega_{x,y} = -\frac{12e_p^2}{25} + \frac{\epsilon_r + 3e_p^2 - 2}{5[1 + (\epsilon_r - 1)L_{x,y}]} \quad (40)$$

Thus, by simple replacing β_i by α_i as given in Equations 38–40, we have an analytical solution for the IEA approximation to calculate the surface- and orientation-averaged SERS EFs.

3 | RESULTS AND DISCUSSION

3.1 | T-matrix simulations

The accuracy of the EA and IEA approximations was evaluated by comparing them to T-matrix simulations of the extinction spectra and SERS EFs of spheroidal particles. These were calculated using publicly available codes (SMARTIES)^[27] with $n = 15$ multipoles, all m 's $[-(2n+1) \leq m \leq 2n+1]$, and 80 points for the theta-quadrature. We used experimental particle width of $2a = 26$ nm,^[10] a constant refractive index of 1.334 for water, and Johnson and Christy^[32] data for the dielectric function of gold. Surface-averaged quantities were calculated by using a rectangular quadrature of 360 angles θ and analytical averaging for azimuth φ (see below for details). For orientation averaging, the SERS EFs were averaged using a 31-point Gaussian quadrature for theta (the results are independent of phi). For each incident direction, the SERS EFs are calculated for two orthogonal polarizations, but the polarization averaging is not trivial and explained in what follows.

We consider a fixed incident direction and assume we have found the full solution of the problem for two orthogonal incident polarization vectors denoted \mathbf{E}_1^0 and \mathbf{E}_2^0 . We denote \mathbf{E}_1 and \mathbf{E}_2 these solutions. Note that although the incident polarizations were orthogonal, the corresponding solutions may not be. The most general incident polarization is of the form $\mathbf{E}^0 = \mathbf{E}_1^0 \cos\gamma + \mathbf{E}_2^0 \sin\gamma$, and the corresponding solution is $\mathbf{E} = \mathbf{E}_1 \cos\gamma + \mathbf{E}_2 \sin\gamma$. We can therefore perform polarization-averaging by averaging over γ chosen uniformly between 0 and 2π . By construction, the result should be independent of the choice of \mathbf{E}_1^0 and \mathbf{E}_2^0 . Let us first consider the field intensity. After expanding and averaging over γ , we obtain the standard result: $\langle |\mathbf{E}|^2 \rangle_\gamma = \frac{1}{2}(|\mathbf{E}_1|^2 + |\mathbf{E}_2|^2)$. The same applies to all quantities that are quadratic in the fields and therefore to absorption, extinction, and scattering cross sections. The situation is more complicated for SERS EFs, which are quartic properties. Let us consider the general case: $EF = |\mathbf{E}^L|^2 |\mathbf{E}^R|^2$, where \mathbf{E}^L and \mathbf{E}^R are short notations for $\mathbf{E}(\omega_L)$ and $\mathbf{E}(\omega_R)$. After expanding and averaging over γ , we obtain

$$\begin{aligned} \langle |\mathbf{E}^L|^2 |\mathbf{E}^R|^2 \rangle_\gamma &= \frac{3}{8} \left(|\mathbf{E}_1^L|^2 |\mathbf{E}_1^R|^2 + |\mathbf{E}_2^L|^2 |\mathbf{E}_2^R|^2 \right) + \frac{1}{2} \operatorname{Re} [\mathbf{E}_1^L (\mathbf{E}_2^L)^*] \operatorname{Re} [\mathbf{E}_1^R (\mathbf{E}_2^R)^*] \\ &\quad + \frac{1}{8} \left(|\mathbf{E}_1^L|^2 |\mathbf{E}_2^R|^2 + |\mathbf{E}_2^L|^2 |\mathbf{E}_1^R|^2 \right). \end{aligned} \quad (41)$$

For the full orientation averaging, one can then average this expression over all possible incident directions. For axisymmetric particles, this reduces to averaging over a single angle. Surface-averaging can also be carried out

and is much faster and more accurate if the averaging over azimuthal angle φ is carried out analytically as pointed out in Somerville et al.^[27] To apply it to the expression above, the method detailed in Somerville et al.^[27] must be generalized to expressions of the form $\langle \operatorname{Re}[XY^*] \operatorname{Re}[ZU^*] \rangle_S$ (all terms in the equation can be expressed in this form). The starting point is the same: all quantities within the T-matrix formalism can be expressed as a sum over azimuthal quantum number, where the φ -dependence is given analytically, for example (for a maximum of N multipoles):

$$X(\theta, \varphi) = \sum_{m=-N}^N X_m(\theta) e^{im\varphi} \text{ and } Y(\theta, \varphi) = \sum_{m=-N}^N Y_m(\theta) e^{im\varphi} \quad (42)$$

Rearranging the double sum, we deduce

$$\operatorname{Re}[XY^*] = \sum_{q=-2N}^{2N} Z_q(\theta) e^{iq\varphi}, \text{ with } Z_q = \begin{cases} \sum_{m=-N+q}^N X_m Y_{m-q}^*, & (q \geq 0), \\ \sum_{m=-N}^{N+q} X_m Y_{m-q}^*, & (q \leq 0). \end{cases} \quad (43)$$

We then follow the method of Somerville et al.^[27] to compute surface averages of the form $\langle AB \rangle_S$. Guided by the expression above, we start from

$$A(\theta, \varphi) = \sum_{q=-2N}^{2N} A(\theta) q e^{iq\varphi} \text{ and } B(\theta, \varphi) = \sum_{q=-2N}^{2N} B(\theta) q e^{iq\varphi}.. \quad (44)$$

Taking the product, and averaging over φ using $\langle e^{ip\varphi} \rangle = \delta_{0p}$, we then deduce

$$\langle AB \rangle_S = \sum_{q=-2N}^{2N} \langle A_q(\theta) B_q^*(\theta) \rangle_\theta. \quad (45)$$

3.2 | Surface integral equation simulations

For gold nanocigars, the SIE method^[28] was used to calculate the local electric field and SERS EFs with specially developed (and tested) codes for plasmonic and metallic nanoparticles.^[29] The calculation details are described in Khlebtsov et al.^[10] For a given incident excitation, the local fields were calculated at both the laser excitation and Raman wavelengths and then surface-averaged to calculate $\langle |\mathbf{E}_L|^2 |\mathbf{E}_R|^2 \rangle_S$. Finally, the

orientation-averaged EFs were obtained by averaging the results over 1,000 random incident orientation-polarization excitations. This was not much more costly than the calculations for a given excitation geometry because the SIE interaction matrix is independent of incident excitation.

3.3 | Extinction and absorption spectra in EA and IEA approximations

Figure 2a,b shows the extinction and absorption spectra of randomly oriented spheroids. Note that the extinction and absorption cross sections are calculated by known formulae for small spheroids^[25] using the corresponding EA and IEA polarizabilities. The EA plots in Figure 2a illustrate larger and blue shifted extinction LPR peaks compared with the T-matrix calculations.

The EA overestimation of the extinction seems related to the incorrect scattering contribution because the absorption peak heights are in reasonable agreement with those calculated by T-matrix method (Figure 2b). In terms of peak position, it is clear that the T-matrix predictions are red-shifted compared with the EA extinction as illustrated in Figure 2c for aspect ratio ranging from 2 to 6. This is well documented and attributed to retardation and radiation damping.

Figure 3 displays the same set of plots but now for the IEA. The agreement is very good, to the point that one cannot see the dashed lines, but there is a tiny difference when we zoom in. Note one discrepancy: the IEA does not predict the expected quadrupole peak^[26] for the highest aspect ratio since by construction it only considers the dipolar response of the particle.

We conclude that the IEA gives excellent agreement with exact T-matrix calculations at least for particle

length (52–156 nm) and aspect ratios 2–6 considered here, which correspond to volume-equivalent diameters between 32 and 47 nm. Note that typical nanorod width is less than 20 nm,^[12] except for special synthesis in a binary surfactant mixture.^[13,33] Also, the upper limit of aspect ratios is typically less than 6, and the longitudinal LPR wavelength is also less than 1,000 nm.^[11,34,35] This means that the IEA can be used for accurate prediction of far-field cross sections for small gold spheroids.

3.4 | SERS enhancement factors in EA and IEA approximations

We now consider a SERS experiment, where the SERS EF of a given Raman peak is compared for the different particles. To match our own experimental results (see later), we set the excitation wavelength at 785 nm, and the Raman-shifted wavelength at 877 nm Raman, which corresponds to the relative Raman frequency shift $(\omega_L - \omega_R)/\omega_L = 0.105$ or $1,342 \text{ cm}^{-1}$ in terms of the wave number Raman shift. We study the intensity (EF) for this Raman peak under different approximation in the EA and IEA, compared with the exact T-matrix result.

In Figure 4, we compare three surface- and orientation-averaged enhancement factors $\langle |E_L|^4 \rangle$, $\langle |E_R|^4 \rangle$, and $\langle |E_L|^2 |E_R|^2 \rangle$ calculated by the T-matrix and EA methods. The simulated results are plotted against aspect ratio (Figure 4a) and also against LPR wavelength (Figure 4b). The agreement between the approximate and exact calculations is poor for EF versus AR plots in both peak positions and peak magnitudes. However, for the EF as a function of the LPR wavelength, the standard EA gives a reasonable estimate of the spectral position of the EF peaks but overestimates the peak values.

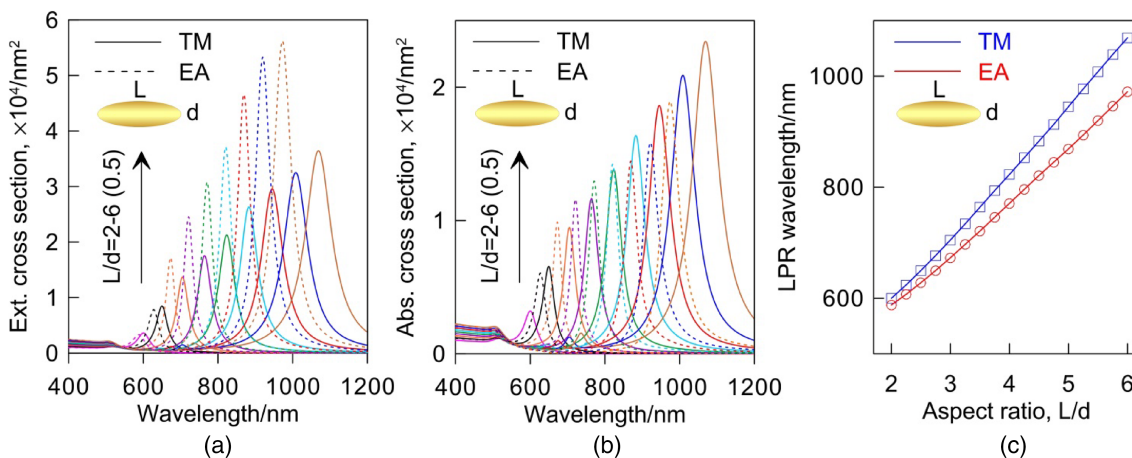


FIGURE 2 Extinction (a) and absorption (b) spectra and LPR peak position (c) calculated by T-matrix method (TM, solid lines) and common electrostatic approximation (EA, dashed lines) for Au spheroids with thickness of 26 nm and aspect ratio ranging from 2 to 6

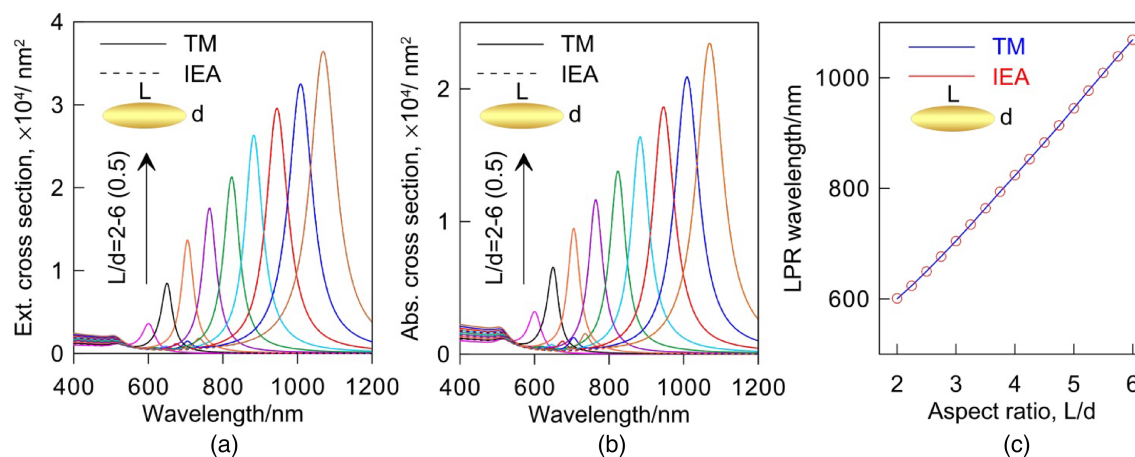


FIGURE 3 Same as in Figure 2 but for T-matrix (TM) and improved electrostatic approximation (IEA). The solid (T-matrix) and dashed (IEA) lines are indistinguishable

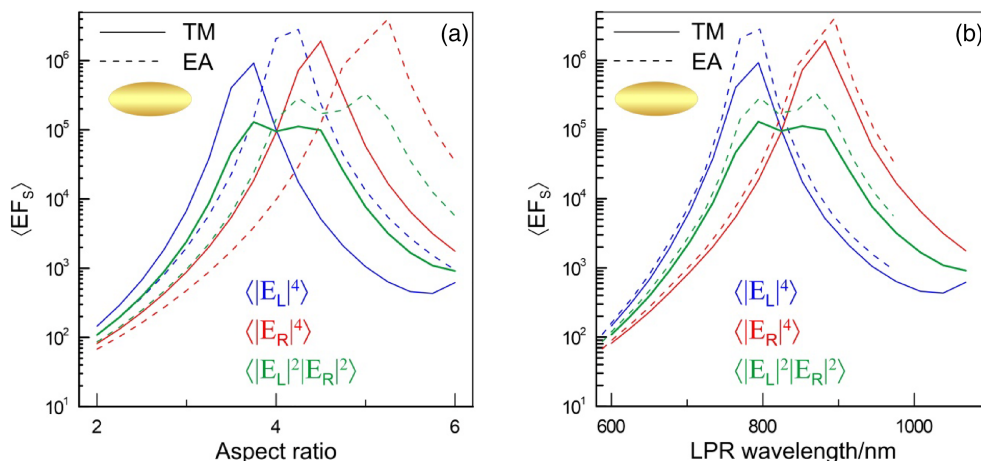


FIGURE 4 Orientation- and surface-averaged SERS EFs of Au spheroids as a function of the aspect ratio (a) and the LPR wavelength (b). Simulations for spheroid width $d = 2b = 26$ nm by the T-matrix method (TM, solid lines) and common electrostatics approximation (EA, dashed lines), using the fourth-power approximation for the laser wavelength (785 nm, blue), Raman-shifted wavelength (877 nm, red), and the full Equation 1 (green)

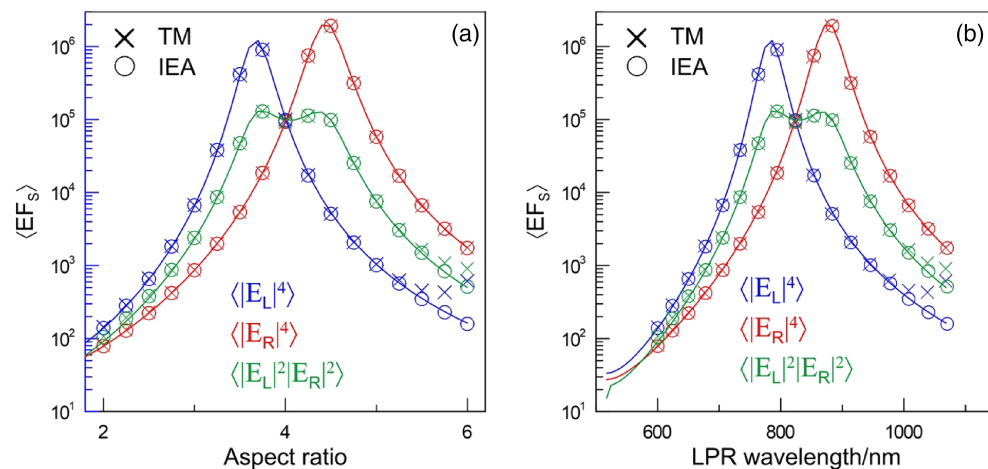
Figure 5 is the same as Figure 4, now for the IEA. First of all, there is again excellent agreement between the exact T-matrix plots and those calculated with the IEA for EFs plotted against the aspect ratio and LPR wavelength. The agreement is almost perfect, except when the aspect ratio is the largest. The LPR there is above 1,000 nm, and the quadrupole peak (down at 700 nm) starts to contribute to the EF at 785 nm. Because the IEA has only a dipole term, it is normal that the IEA does not predict that effect.

Another important result is that the T-matrix and IEA simulations with the full Equation 1 predict small EF variations around about 10^5 for PR wavelengths between 800 nm and 900 nm (the corresponding aspect ratios are between 3.5 and 4.5). That is what was observed in our measurements^[10] for AuNRs whose PR

was above the excitation wavelength. With increasing AuNR aspect ratio and PR wavelength, the predicted SERS EF starts to decrease, in agreement with the experimental data for long nanorods.^[10] However, for aspect ratios smaller than 3.5 or, equivalently, for PRs below the excitation wavelength, the simulated EFs decrease by almost three orders of magnitude, in drastic contrast with the experimental data. This point has been discussed in Khlebtsov et al.^[10]

Yet another important conclusion is that the widely used zero-shift four-power law gives incorrect estimates of the SERS EFs—even when surface and orientation averaging is taken into account ($EFE_S = \langle \langle |\mathbf{E}_{loc}(w_L)|^4 \rangle_S \rangle$). The calculated EF dependences on the PR wavelength have a narrow-width peak centered at the laser excitation wavelength (blue plot in Figure 5b) or at the

FIGURE 5 Orientation- and surface-averaged SERS EFs of Au spheroids as a function of the aspect ratio (a) and the PR wavelength (b). Simulations for spheroid width $d = 2b = 26$ nm by the T-matrix method (TM, crosses) and improved electrostatics approximation (IEA, circles), by using the fourth-power approximation for the laser wavelength (785 nm, blue), Raman-shifted wavelength (877 nm, red), and the full Equation 1 (green)



Raman-shifted wavelength, corresponding to $\langle\langle|\mathbf{E}_{loc}(\omega_R)|^4\rangle_S\rangle$ (red plot in Figure 5b). When the full Equation 1 is used for simulations, the integrand product of the local intensities $|\mathbf{E}_{loc}(\omega)|^2|\mathbf{E}_{loc}(\omega_R)|^2$ has a flatter behavior, and no strong resonance is observed near the laser wavelength (green plot in Figure 5b).

Finally, in Figure 5, calculated EFs are almost 5 times higher than that measured experimentally for cigar-like nanorods of similar thickness (24–26 nm) and LPR wavelength ranging from 925 to 650 nm. To verify whether this difference is related to the spheroidal model, we did additional simulations with cigarlike AuNRs. The local fields were calculated by the surface integral equation (SIE) method^[28] and then surface and orientation averaging was done with Equation 1.

Figure 6 shows the surface- and orientation-averaged local fields $\langle|E_{loc}|^4\rangle$ for the laser and Raman-shifted wavelengths ω_L and ω_R , respectively, as a function of the aspect ratio of nanospheroids (T-matrix calculations) and nanocigars (SIE calculations). There is a small shift in the peak position between cigars and spheroids, as also observed previously.^[36] Because of the resonance behavior of the $\langle|E_L|^4\rangle$ and $\langle|E_R|^4\rangle$ quantities and because of the notable difference in their peak position, the fourth-power law strongly overestimates the EF, as compared with the SERS EF calculated with Equation 1. The average cigar EFs are also reduced, as compared with those of spheroids because of the reduced curvature at the tip. But as for spheroids, there is a flat portion of the full EF $\langle|E_L|^2|E_R|^2\rangle$ as a function of the LPR wavelength. For wavelengths between 785 and 900 nm, SIE simulations (green line) agree with the averaged experimental data^[10] for gold cigars. However, there is still a strong disagreement between simulations and measurements for shorter and longer wavelengths. This point is discussed in Khlebtsov et al.^[10]

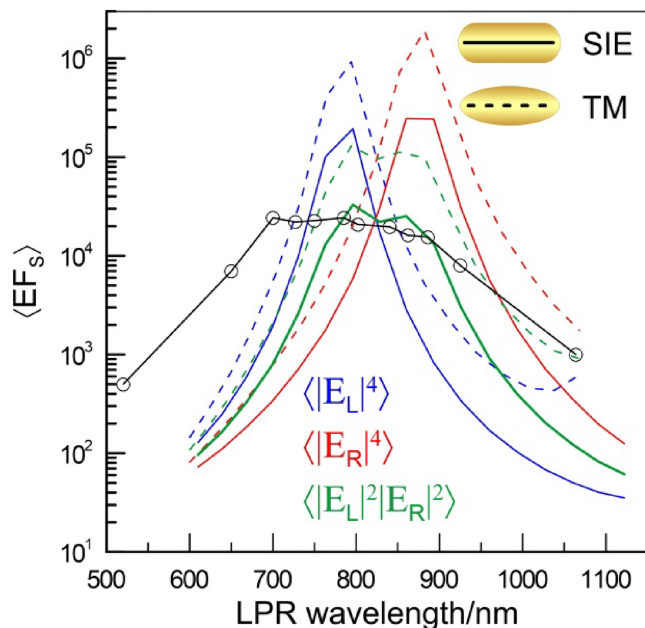


FIGURE 6 Orientation- and surface-averaged local fields for the laser wavelength ($\langle|E_L|^4\rangle$, blue curves), the Raman-shifted wavelength ($\langle|E_R|^4\rangle$, red curves), and the SERS EF ($\langle|E_L|^2|E_R|^2\rangle$, green curves) as a function of the aspect ratio. Calculation by the T-matrix method for nanospheroids (TM, dashed lines) and by the SIE method for nanocigars (SIE, solid lines). Black circles show the averaged experimental data of Khlebtsov et al.^[10] for gold cigars and 30-nm nanospheres (at 520 nm)

4 | CONCLUSION

We have obtained an explicit analytical solution to the surface- and orientation-averaged SERS EF for randomly oriented prolate spheroidal particles in the common (EA) and improved (IEA) electrostatic approximations. The solution involves two decomposition coefficients $a(\omega)$ and $b(\omega)$ of local electromagnetic field on the

spheroid surface. These coefficients are expressed through the usual electrostatic polarizabilities β_i in EA and generalized IEA polarizabilities α_i , which account for size-dependent radiative damping, depolarization effects, and interactions with higher order multipoles. We have demonstrated perfect agreement between the IEA and the T-matrix calculations for far-field cross sections and near-field SERS EFs, except for high aspect ratios where the quadrupolar resonance becomes more important. This approach can easily be generalized to oblate spheroids as the improved polarizabilities in Equations 38–40 are also valid for oblate spheroids.^[26]

Calculations for gold nanocigars of the same thickness as for spheroids show that the spheroidal model gives overestimated SERS EFs because of the higher curvature at the tip. To improve our solution and make it applicable for real AuNRs, it is possible, at least in principle, to consider the lowest-order T-matrix elements for cigar-like particles similarly to derivation of Majic et al.^[26] In the first approximation, this would give an effective electrostatic polarizability tensor of small plasmonic cigars as a function of their aspect ratio, whereas higher size-dependent terms would include radiation damping and other effects. In addition, one would have to generalize the decomposition (Equation 12) for cigars. Then, our analytical solution could be generalized for other axially symmetrical particles by simply replacing the decomposition coefficients $a(\omega)$ and $b(\omega)$ of spheroids with their counterparts. Another interesting extension of this study would be to consider the important case of a dimer of sphere.^[37] For this, it will be necessary to derive low-order approximations of the superposition T-matrix method.^[38,39]

ACKNOWLEDGEMENTS

This research was supported by the Russian Scientific Foundation (project no. 18-14-00016). The experimental part of research was supported by grants from the Russian Foundation of Basic Research (project no. 18-52-7803).

CONFLICT OF INTEREST

None.

ORCID

Nikolai G. Khlebtsov  <https://orcid.org/0000-0002-2055-7784>

REFERENCES

- [1] E. C. Le Ru, P. G. Etchegoin, *Annu. Rev. Phys. Chem.* **2012**, 63, 65.
- [2] M. Fleischmann, P. J. Hendra, A. J. MsQuillan, *Chem. Phys. Lett.* **1974**, 26, 163.
- [3] D. L. Jeanmarie, R. P. Van Duyne, *J. Electroanal. Chem.* **1977**, 84, 1.
- [4] M. G. Albrecht, J. A. Creighton, *J. Am. Chem. Soc.* **1977**, 99, 5215.
- [5] Y. Wang, B. Yan, L. Chen, *Chem. Rev.* **2013**, 113, 1391.
- [6] J. Langer, D. J. de Aberasturi, J. Aizpurua, et al., *ACS Nano* **2020**, 14, 28.
- [7] J. Zhao, J. A. Dieringer, X. Zhang, G. C. Schatz, R. P. Van Duyne, *J. Phys. Chem. C* **2008**, 12, 19302.
- [8] G. C. Schatz, *Acc. Chem. Res.* **1984**, 17, 370.
- [9] G. C. Schatz, *Acc. Chem. Res.* **1984**, 17, 370. In: K. Kneipp, M. Moskovits, H. Kneipp (Eds), *Surface-Enhanced Raman Scattering—Physics and Applications*, Vol. 2006, Springer, Berlin 19.
- [10] B. N. Khlebtsov, V. A. Khanadeev, A. M. Burov, E. C. Le Ru, N. G. Khlebtsov, *J. Phys. Chem. C* **2020**, 124, 10647.
- [11] H. Chen, L. Shao, Q. Li, J. Wang, *Chem. Soc. Rev.* **2013**, 42, 2679.
- [12] L. Vigderman, B. P. Khanal, E. R. Zubarev, *Adv. Mater.* **2012**, 24, 4811.
- [13] B. N. Khlebtsov, V. A. Khanadeev, J. Ye, G. B. Sukhorukov, N. G. Khlebtsov, *Langmuir* **2014**, 30, 1696.
- [14] J. Rodríguez-Fernández, G. Pérez-Juste, P. Mulvaney, L. M. Liz-Marzán, *J. Phys. Chem. B. (Letter)* **2005**, 109, 14257.
- [15] V. A. Khanadeev, N. G. Khlebtsov, A. M. Burov, B. N. Khlebtsov, *Colloid J.* **2015**, 77, 652.
- [16] S. T. Sivapalan, B. M. De Vetter, T. K. Yang, T. van Dijk, M. V. Schulmerich, P. S. Carney, R. Bhargava, C. J. Murphy, *ACS Nano* **2013**, 7, 2099.
- [17] K.-Q. Lin, J. Yi, J.-H. Zhong, S. Hu, B.-J. Liu, J.-Y. Liu, C. Zong, Z.-C. Lei, X. Wang, J. Aizpurua, R. Esteban, B. Ren, *Nat. Commun.* **2017**, 8, 14891.
- [18] M. Kerker, D.-S. Wang, H. Chew, *Appl. Opt.* **1980**, 19, 4159.
- [19] E. C. Le Ru, P. G. Etchegoin, *Chem. Phys. Lett.* **2006**, 423, 63.
- [20] L. K. Ausman, G. C. Schatz, *J. Chem. Phys.* **2009**, 131, 084708.
- [21] E. C. Le Ru, P. G. Etchegoin, *Principles of Surface Enhanced Raman Spectroscopy and Related Plasmonic Effects*, Elsevier, Amsterdam **2009**.
- [22] E. C. Le Ru, M. Meyer, E. Blackie, P. G. Etchegoin, *J. Raman Spectrosc.* **2008**, 39, 1127.
- [23] E. C. Le Ru, J. Grand, N. Félidj, J. Aubard, G. Lévi, A. Hohenau, J. R. Krenn, E. Blackie, P. G. Etchegoin, *J. Phys. Chem. C (Letter)* **2008**, 112, 8117.
- [24] M. Kerker, *J. Colloid Interface Sci.* **1987**, 118, 417.
- [25] C. F. Bohren, D. R. Huffman, *Absorption and Scattering of Light by Small Particles*, Wiley, New York **1983**.
- [26] M. Majic, L. Pratley, D. Schebarchov, W. R. C. Somerville, B. Auguie, E. C. Le Ru, *Phys. Rev. A* **2019**, 99, 013853.
- [27] W. R. C. Somerville, B. Auguie, E. C. Le Ru, J. Quant, *Spectrosc. Radiat. Transfer* **2016**, 174, 39.
- [28] A. M. Kern, O. J. F. Martin, *J. Opt. Soc. Am. A* **2009**, 26, 732.
- [29] T. V. Raziman, W. R. C. Somerville, O. J. F. Martin, E. C. Le Ru, *J. Opt. Soc. Am. B* **2015**, 32, 485.
- [30] M. I. Mishchenko, L. D. Travis, A. A. Lacis, *Scattering, Absorption, and Emission of Light by Small Particles*, Cambridge Univ. Press, Cambridge, UK **2002**.
- [31] E. C. Le Ru, W. R. C. Somerville, B. Auguie, *Phys. Rev. A* **2013**, 87, 012504.
- [32] P. B. Johnson, R. W. Christy, *Phys. Rev. B* **1972**, 6, 4370.

- [33] X. Ye, C. Zheng, J. Chen, Y. Gao, C. B. Murray, *Nano Lett.* **2013**, *13*, 765.
- [34] A. V. Alekseeva, V. A. Bogatyrev, B. N. Khlebtsov, A. G. Mel'nikov, L. A. Dykman, N. G. Khlebtsov, *Colloid J.* **2006**, *68*, 661.
- [35] L. A. Dykman, N. G. Khlebtsov, *Chem. Soc. Rev.* **2012**, *41*, 2256.
- [36] N. G. Khlebtsov, L. A. Trachuk, A. G. Melnikov, *Proc. SPIE* **2004**, *5475*, 1.
- [37] B. N. Khlebtsov, A. G. Melnikov, V. P. Zharov, N. G. Khlebtsov, *Nanotechnology* **2006**, *17*, 1,437.
- [38] B. Peterson, S. Ström, *Phys. Rev. D* **1973**, *8*, 3661.
- [39] D. Schebarchov, E. C. Le Ru, J. Grand, B. Auguié, *Optics Express* **2019**, *27*, 35750.

How to cite this article: Khlebtsov NG, Le Ru EC. Analytical solutions for the surface- and orientation-averaged SERS enhancement factor of small plasmonic particles. *J Raman Spectrosc.* 2021; **52**:285–295. <https://doi.org/10.1002/jrs.5980>